Experimental verification of spatially varying fracture-compliance estimates obtained from AVO inversion coupled with linear slip theory

Minato, Shohei; Ghose, Ranajit; Osukuku, Godfred

DOI
10.1190/geo2017-0069.1

Publication date
2017

Document Version
Final published version

Published in
Geophysics

Citation (APA)
Minato, S., Ghose, R., & Osukuku, G. (2017). Experimental verification of spatially varying fracture-compliance estimates obtained from AVO inversion coupled with linear slip theory. *Geophysics*, *83 (2018)*(1), WA1-WA8. https://doi.org/10.1190/geo2017-0069.1

GEOPHYSICS, VOL. 83, NO. 1 (JANUARY-FEBRUARY 2018); P. WA1–WA8, 9 FIGS.
10.1190/GEO2017-0069.1

Experimental verification of spatially varying fracture-compliance estimates obtained from amplitude variation with offset inversion coupled with linear slip theory

Shohei Minato[1], Ranajit Ghose[1], and Godfred Osukuku[1]

ABSTRACT

The elastic compliance of a fracture can be spatially varying, reflecting the variation of microscale properties of the fracture, e.g., aperture, contact asperities, and fracture infill. Characterizing the spatial heterogeneity of a fracture is crucial in explaining the apparent frequency dependence of fracture compliance and in addressing the spatially varying mechanical and hydraulic properties of the fractured medium. Apparent frequency dependence of the estimated fracture compliance is caused when the used seismic wavelength is very large compared to the scale of heterogeneity. We perform ultrasonic laboratory experiments, and characterize the spatially varying compliance along a fluid-filled fracture. We simulate a horizontal fracture, and introduce heterogeneous fluid distribution along the fracture. We perform amplitude variation with offset (AVO) inversion of the P-P reflections, in which we obtain the theoretical angle-dependent reflection responses by considering the linear-slip model. The estimated compliance distribution clearly separates the dry region from the wet region of the fracture. The effective bulk modulus of the fluid is estimated using the derived values of the compliance. We find that the obtained bulk modulus is well-explained by the presence of minute quantity of air bubbles in the water. We also find new evidence of the existence of scattered waves generated at the boundary representing a sharp change in fracture compliance. The estimated boundary between the dry and the wet regions of the fracture, which is detected by AVO inversion, is slightly shifted compared with the actual location. This is possibly due to the interference of the scattered waves that are generated at the boundary. The linear-slip model can represent thin structures in rocks in a wide range of scale. Therefore, our methodology, results, and discussion will be useful in developing new applications for assessing laterally varying mechanical and hydraulic properties of thin nonwelded discontinuities, e.g., fractures, joints, and faults.

INTRODUCTION

Elastic-wave responses of fractured rocks are often represented by the linear-slip model (Schoenberg, 1980). The model considers a fracture to be an imperfect interface across which the seismic stress $\mathbf{t}$ is continuous but the displacement $\mathbf{u}$ is discontinuous:

$$\Delta\mathbf{u} = \mathbf{Z}\mathbf{t}, \tag{1}$$

where the compliance matrix $\mathbf{Z}$ contains the normal compliance η_N and the tangential compliance η_T. The elastic compliances of a fracture are controlled by microscale properties, e.g., aperture, contacting asperities, and fracture infill materials (Liu et al., 1995; Hudson et al., 1997). The fracture compliances are also sensitive to the stress field and fluid flow properties (Hopkins et al., 1987; Pyrak-Nolte and Morris, 2000). The linear-slip model represents wave propagation across a thin structure in a wide range of scale. Therefore, it is useful in laboratory estimation of compliance of rock fractures (Pyrak-Nolte et al., 1990; Lubbe et al., 2008), in representation of rock joints and rough surfaces in metals (Nagy, 1992; Lavrentyev and Rokhlin, 1998), and in monitoring geologic faults (Worthington and Hudson, 2000; Kame et al., 2014).

The microscale properties of natural fractures are spatially heterogeneous along the fracture surface. Nakagawa et al. (2004) point out that a variety of microstructures can be modeled considering heterogeneous fracture compliance, e.g., the heterogeneous

Manuscript received by the Editor 31 January 2017; revised manuscript received 16 May 2017; published ahead of production 13 September 2017; published online 14 November 2017.
[1]Delft University of Technology, Department of Geoscience and Engineering, Delft, The Netherlands. E-mail: s.minato-1@tudelft.nl; r.ghose@tudelft.nl; godfredosukuku@gmail.com.

distribution of microcracks, partial contacts, and soft materials in a fracture. Previous laboratory experiments using elastic waves show the evidence of the spatially varying nature of the fracture compliance due to mineral precipitation and/or stress distribution along the fracture plane (Oliger et al., 2003; Acosta-Colon et al., 2009). Furthermore, it is known that a seismic wavelength that is too large to resolve spatial heterogeneity in fracture compliance results in the apparent frequency dependence of the compliance (Pyrak-Nolte and Nolte, 1992; Baird et al., 2013). Therefore, characterizing the lateral variation of the fracture compliance is quite important to estimate the spatially heterogeneous mechanical and hydraulic properties of the fractured medium.

In this study, we use reflected waves from a single fracture to characterize the laterally varying fracture compliance. We consider elastic waves that have a wavelength that is much larger than the thickness of a fracture and also much larger than the spacing between the contact asperities but much shorter than the lateral extent of the fracture. In this case, Hudson's theory (Worthington and Hudson, 2000; Worthington and Lubbe, 2007) indicates that the fluid distribution will be dominant in causing the heterogeneous compliance of a fracture that has a spatially invariant statistical properties for the contacting asperities.

Most field seismic measurements of fracture compliances exploit the effective medium theory (Bakulin et al., 2000), which characterizes an assembly of relatively small fractures that are individually invisible in a given scale of seismic measurement. However, recent studies on fractures of a scale larger than or comparable with the seismic wavelength show the evidence of reflections from a single fracture (Reshetnikov et al., 2010), or scattered waves due to multiple fractures (Willis et al., 2006). These large-scale fractures can have a dominant effect on the mechanical and hydraulic properties of the subsurface (Aydin, 2000; Lee et al., 2001). Therefore, exploring for a method that can accurately estimate the laterally varying compliance of a single fracture is worthwhile in many different applications, e.g., in monitoring cracks, joints, or faults. To achieve this goal, a high-resolution, nonlinear imaging condition (Minato and Ghose, 2015) and inverse scattering approaches (Minato and Ghose, 2014, 2016b) have recently been proposed for fracture imaging and characterization.

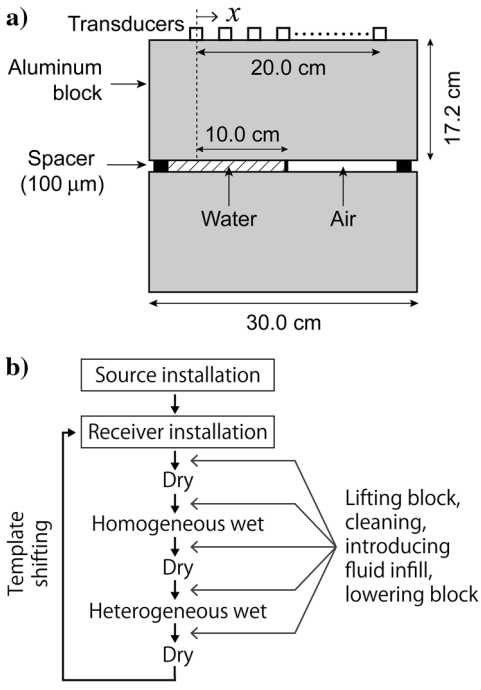

Figure 1. (a) Experimental setup for measuring the reflection responses from a spatially heterogeneous, horizontal fracture and (b) the measurement procedure.

To obtain the fracture compliances, the use of angle-dependent reflection coefficients (amplitude variation with offset [AVO]) from a fracture has recently been proposed (Minato and Ghose, 2016a). Minato and Ghose (2016a) use aluminum blocks to simulate a horizontal fracture, and they successfully estimate the compliance of a water-filled fracture, assuming homogeneous (laterally invariant) distribution of water. In conventional AVO inversion, one estimates the local impedance contrast across the boundary (welded contact) between two geologic layers (Shuey, 1985). On the contrary, a fracture represents a nonwelded contact. The angle-dependent reflection coefficients at a fracture are represented by the linear-slip model, and they are frequency dependent (Schoenberg, 1980; Chaisri and Krebes, 2000). Therefore, the AVO inversion of a fracture is designed in the frequency domain (Minato and Ghose, 2016a).

In this study, we perform laboratory experiments and obtain angle-dependent reflection responses from a fracture with laterally varying compliance. To create laterally varying (heterogeneous) compliance, we consider a simple case in which a dry (air-filled) fracture changes to a wet (water-filled) condition. In reality, a distribution of many such changes can be tackled by the approach developed in this research. We create an artificial fracture using aluminum blocks. We introduce spatial heterogeneity in fluid distribution along the fracture. Considering surface seismic measurements or borehole measurements involving multiple sources and receivers, the possibility of AVO inversion of common midpoint (CMP) gathers is explored. Note that for a fracture with laterally/spatially heterogeneous compliance distribution, the presence of scattered waves is earlier predicted numerically (Nakagawa et al., 2004). We detect, for the first time, the evidence of scattered waves from the fracture heterogeneity in an experimental data set. The effects of these scattered waves on the compliance estimation by AVO inversion are discussed.

EXPERIMENT SETUP

We use two aluminum blocks to simulate a horizontal fracture in a rock (Figure 1a). A spacer of known thickness (100 μm) is installed to determine the aperture of the artificial fracture. The state of the fracture infill, i.e., wet (a water-filled fracture) or dry (an air-filled fracture), is affected by lifting the top aluminum block, cleaning and introducing the fluid at the fracture surface, and then carefully lowering the top block to the original position. Minato and Ghose (2016a) use the same experimental setup and estimate the homogeneous fracture compliances of a water-filled fracture using AVO analysis. In this study, we introduce lateral heterogeneity in the fluid distribution along the fracture by creating a wet region (filled with a mixture of water and hair gel) and a dry region (filled with air) along the fracture (see Figure 1a). The two regions are separated by a thinly cut polypropylene-based adhesive tape (approximate width of 0.2 mm and thickness of 100 μm) placed at $x = 10$ cm. Note that to increase the fluid viscosity, we use a mixture of water and hair gel (see the "Discussion" section for details), assuming the hair gel to have a similar bulk modulus to that of water (Leroy et al., 2008). We use longitudinal transducers (Panametrics V103) for measuring

P-P reflections. The center frequency of the generated source signal is 1.0 MHz. The predominant frequency of the observed reflection event is approximately 0.7 MHz.

Figure 1b shows the measurement procedure. We simulate surface seismic measurements for a horizontal fracture by using a fixed receiver array observing the elastic waves due to a source located at multiple positions at the surface. Note that when we rotate this acquisition geometry, it represents borehole measurements for a (sub) vertical fracture with sources and receivers positioned in a borehole. Therefore, the experiments can also be interpreted as borehole measurements to characterize subvertical fractures.

We use a template to accurately locate the receiver transducers, and we then repeatedly shift the template to simulate a receiver array ("template shifting" in Figure 1b). At the fixed source-receiver configuration, we measure three dry responses and two wet responses (Figure 1b). The dry response represents that the fracture is homogeneously filled with air; the two wet responses represent the situation when the fracture is homogeneously filled with water and one when the fracture is heterogeneously filled with water and air, i.e., a spatially varying fracture (see Figure 1a). Here, we confirm that the water does not leak into the dry region during the measurement of the heterogeneously wet response by visually inspecting the fracture surface when the block is lifted (Figure 1b). The three dry responses are used to calculate the reflection coefficients of the wet fracture and to evaluate any changes in coupling during the experiments (see also Minato and Ghose, 2016a). We achieve a source spacing of 1 cm and a receiver spacing of 5 mm along a 20 cm long survey line (Figure 1a). Due to the finite dimension of the transducers, the minimum source-receiver offset is 2.5 cm.

The AVO analysis and the reproducibility tests using six different incidence angles for the reflected waves, which use the same artificial fracture and a spatially homogeneous distribution of fluid, are discussed in detail by Minato and Ghose (2016a). Following the results in Minato and Ghose (2016a), we assume that the fracture has a smooth surface without asperities. In this case, considering the quasistatic approximation, which assumes the wavelength to be much larger than the fracture aperture (Nagy, 1992), the fracture compliances are determined by the fracture aperture d and the bulk modulus of the infill fluid K_f, i.e., $\eta_N^{-1} \approx K_f/d$ and $\eta_T^{-1} \approx 0$. We assume the elastic properties of the aluminum blocks as $V_P = 6400$ m/s, $V_S = 3150$ m/s, and $\rho = 2700$ kg/m^3.

In the present experiments, we consider a laboratory analog for surface seismic measurements or borehole measurements, to characterize a 20 cm long fracture with fracture compliance of the order of 10^{-14} m/Pa using ultrasonic frequencies. This order of magnitude of compliance is typical in natural fractures of similar dimensions (Lubbe et al., 2008). As shown in Worthington and Lubbe (2007), fracture compliances show power-law behavior, and low-frequency waves illuminate large structures. In vertical seismic profiling (VSP) measurements with seismic frequencies, Worthington and Hudson (2000) discuss the representation of a large (several kilometers long) geologic fault using the linear-slip model. In microseismic measurements using a borehole, Reshetnikov et al. (2010) show the presence of reflected waves from fractures that have lengths ranging from tens to hundreds of meters. Therefore, it should be possible to perform AVO inversion, as attempted in the present laboratory-scale study, to characterize fractures in the field scales. In the context of the inverse scattering approach, Minato and Ghose (2013) discuss the characterization of heterogeneous fracture compliance considering the relative scales for fracture length, fracture depth, and the correlation length for compliance distribution.

DATA AND ESTIMATED COMPLIANCE DISTRIBUTION

The purpose of this study is to characterize the compliance distribution of the wet fracture using the dry fracture response as a reference. Here, we use the dry fracture responses as the reference, assuming that they are free-surface reflections. For different experiments, however, one may be able to use other responses, e.g., reflected waves with known reflection coefficients. The changes in transducer coupling during the experiments can cause errors in estimating the reflection coefficients (Minato and Ghose, 2016a). Therefore, we evaluate the crosscorrelation coefficients of the observed P-P reflections in consecutive dry responses prior to and after the measurements of the wet responses (see Figure 1b). We assume that the small values of the crosscorrelation coefficients are indicative of small changes in transducer coupling. We then exclude all wet responses whose crosscorrelation coefficients with respect to the dry response at the same source-receiver configuration are less than 0.998.

In this study, we use CMP analysis to characterize the spatial heterogeneity along a fracture. After obtaining all shot gathers, we sort the data into CMP gathers. The CMP spacing is 0.25 cm, and the fold number at each CMP gather is shown in Figure 2a. Here, we present the CMP gathers for the homogeneously wet fracture and those for the heterogeneously wet fracture. The fold numbers and the incidence angles at each CMP gather (Figure 2b) are not symmetrically distributed along the line because of the exclusion of data based on the values of crosscorrelation coefficients, as described above. The incidence angles are calculated from the source and receiver positions, and the known depth of the fracture.

We illustrate the observed P-P reflections from the heterogeneously wet fracture at the wet region (CMP $x = 5$ cm) and at the dry region (CMP $x = 15$ cm) in Figure 3a and 3b, respectively. The red lines in Figure 3 show the responses of the heterogeneously wet fracture, and the black lines show the dry responses. The background color shows the difference between the dry and wet responses. The difference values at the wet region (Figure 3a) indicate that the P-P reflection waveforms at all offsets have been changed due to the inclusion of water. On the other hand, the difference at the dry region (Figure 3b) shows very small values compared with the wet region, which is a clear indication that the reflected waves can distinguish between the wet and the dry regions at the fracture.

We apply the AVO inversion at all CMP gathers and obtain the normal compliance η_N. For this purpose, we assume the fracture compliance to be locally homogeneous at each CMP location. We follow the same approach of Minato and Ghose (2016a): we calculate the reflection coefficients of the heterogeneously wet fracture using the reference responses. Here, we use the average values of consecutive dry responses prior to and after the wet measurements for the reference response. We use the following relation:

$$R_{PP}^{Wet}(\omega,\theta) = R_{PP}^{FS}(\theta)\frac{D^{Wet}(\omega,\theta)}{D^{Dry}(\omega,\theta)}, \tag{2}$$

where R_{PP}^{FS} is the theoretical free-surface P-P reflection coefficient, D^{Dry} is the dry response, D^{Wet} is the wet response, ω is the angular

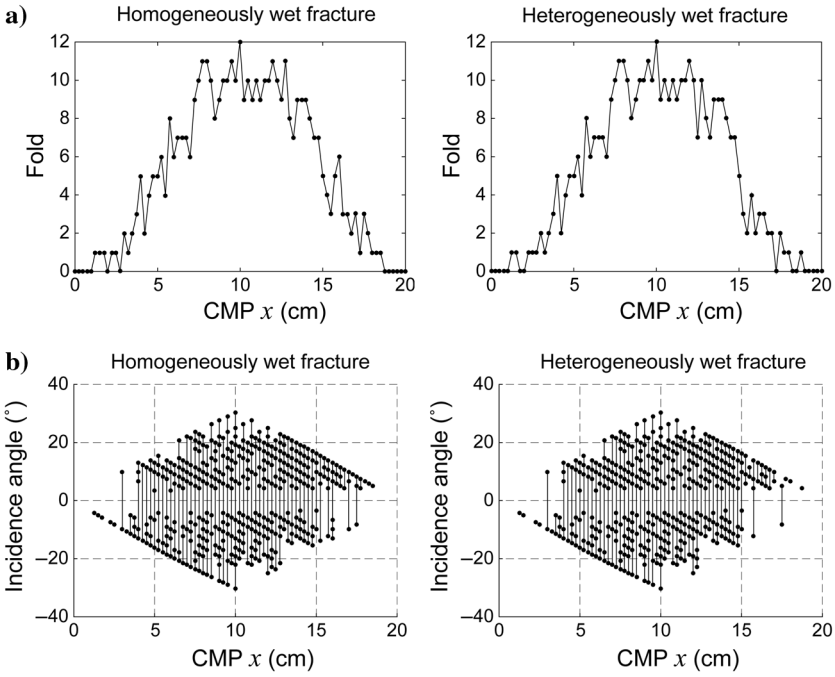

Figure 2. (a) Fold distribution for CMP gathers in case of a homogeneously wet fracture and a heterogeneously wet fracture and (b) incidence angle coverage for the CMP gathers.

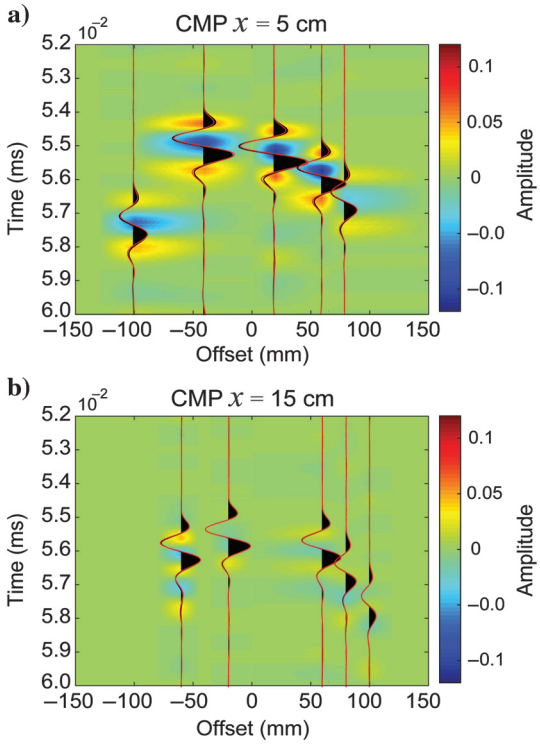

Figure 3. (a) Observed P-P reflections in the CMP gather at the wet region (CMP $x = 5$ cm). See Figure 1a for the x-axis. The response of the heterogeneously wet fracture (red lines), the dry response (black lines), and their difference (background color) are shown and (b) the same as (a) but for the CMP gather at the dry region (CMP $x = 15$ cm).

frequency, and θ is the incidence angle. This procedure compensates for the source directivity, the changes in receiver coupling over the receiver array, and the propagation effect between the source and the receiver (Minato and Ghose, 2016a). The dots in Figure 4 are the calculated reflection coefficients (absolute values) from the CMP gather at the wet region (CMP $x = 5$ cm, Figure 3a). The frequency and angle dependence of the reflection coefficients are conspicuous. The reflection coefficients increase as the frequency increases and the incidence angle decreases, as also shown by Chaisri and Krebes (2000). The solid lines in Figure 4 show the estimated reflection coefficients best fitting the observed coefficients (AVO inversion). Here, we minimize the misfit function $S(\eta_N)$ defined as

$$S(\eta_N) = \frac{\sqrt{\sum_i \sum_j (|R_{PP}^{obs}(\omega_i,\theta_j)| - |R_{PP}^{est}(\omega_i,\theta_j,\eta_N)|)^2}}{\sqrt{\sum_i \sum_j |R_{PP}^{obs}(\omega_i,\theta_j)|^2}}, \quad (3)$$

where $R_{PP}^{obs}(\omega_i,\theta_j)$ and $R_{PP}^{est}(\omega_i,\theta_j,\eta_N)$ are, respectively, the observed and the estimated P-P reflection coefficients for the jth incident angle and the ith frequency component. Here, we assume $\eta_T^{-1} = 0$ when we calculate R_{PP}^{est} using the theoretical P-P reflection coefficients (Schoenberg, 1980; Gu et al., 1996; Chaisri and Krebes, 2000), as discussed in the previous section and in Minato and Ghose (2016a). Figure 5 shows the misfit function (equation 3) of the data shown in Figure 4. We estimate η_N to be 9.4×10^{-14} m/Pa.

We apply this procedure to all CMP gathers and obtain the compliance distribution of the homogeneously wet and heterogeneously wet fracture (Figure 6). One can see that the values of the compliance at the wet region of the heterogeneously wet fracture (between CMP $x = 1$ cm and CMP $x = 10$ cm) very well correspond to those of the homogeneously wet fracture: η_N is estimated to be

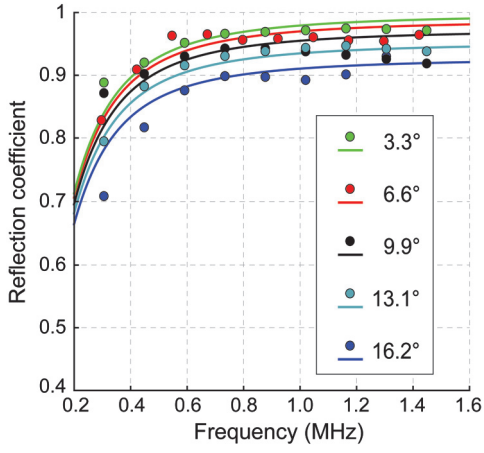

Figure 4. The reflection coefficients for the heterogeneously wet fracture at each incidence angle (absolute value) for the CMP gather at CMP $x = 5$ cm (Figure 3a). The observed coefficients (dots) and the estimated coefficients from the AVO inversion (solid lines) are shown.

8×10^{-14}–10×10^{-14} m/Pa. Furthermore, it is clear that the heterogeneously wet fracture has very high compliance values at the dry region, especially between CMP $x = 12$ cm and CMP $x = 19$ cm (Figure 6). The compliances at the dry region are detected to be 70×10^{-14} m/Pa, which is an upper bound for η_N considered in the inversion (see also Minato and Ghose, 2016a). Note that the apparent boundary between the dry and wet region is shifted at CMP $x =$ 12 cm (the true boundary is located at CMP $x = 10$ cm). This is possibly due to the interference of the scattered waves, which will be discussed in the next section.

Note that, in this analysis, we assume a point source and a point receiver ignoring the dimension of the transducers (13 mm diameter). Although the complex beam-spreading pattern is compensated by the deconvolution procedure (equation 2), the finite dimension of the transducers may affect the choice of the incidence angles in estimating the reflection coefficients and the AVO inversion. Using equation 2, we find that changes in the estimated reflection coefficients at the center frequency, due to different values of the incidence angles considering the dimension of the transducers, are $\pm 0.5\%$ for the smallest incidence angle and $\pm 2.5\%$ for the largest incidence angle.

DISCUSSION

Compliance values of wet fracture

To discuss the estimated compliance values, we first summarize briefly the previous experiments of Minato and Ghose (2016a). In the previous experiments, we use the same experimental setup to obtain fracture compliances of a homogeneously wet fracture. The fracture compliances are obtained using (1) 100 μm thick spacers, (2) 150 μm thick spacers, and (3) without using spacers. The independently repeated tests (error bars in Figure 3 and the supporting information in Minato and Ghose, 2016a) imply the presence of air bubbles. We interpret that the reflection responses without the spacers indicate the presence of a residual aperture due to the long-wavelength discrepancy from the planarity of the fracture surface. Assuming the bulk modulus of water, the fracture apertures are estimated. The fracture compliance and the aperture estimated from the data without using the spacers show better reproducibility than those from the data using the 100/150 μm thick spacers (Figure 3 in Minato and Ghose, 2016a). Therefore, we assume that the residual aperture (approximately 40 μm) obtained from the data without the spacers represents the true residual aperture in which the effect of air bubble is small. Finally, the true aperture, which is obtained as the residual aperture plus the spacer thicknesses (independently measured with an error of ±10 μm), very well explains the estimated values of the apertures in the data using the 100/150 μm thick spacers.

In this study, we obtain the compliance values at the wet region of the fracture to be $\eta_N = 8 \times 10^{-14}$–$10 \times 10^{-14}$ m/Pa (Figure 6). These values are larger than those obtained in the previous experiments ($\eta_N = 6 \times 10^{-14}$–$7 \times 10^{-14}$ m/Pa) by Minato and Ghose (2016a). Between these two experiments, we do not identify any physical damage created on the fracture surface, which implies that the change in the estimated compliance is caused by a change in the relative proportion of water and hair gel. In the present experiments, we increase the amount of hair gel from that of the previous experiments to increase the viscosity of the fluid. We exploit fluid viscosity so that the fluid flows only when the applied stress is larger than the yield stress; viscous fluid is necessary to keep the fluid at a fixed position when lowering the block (see Figure 1b) and to inspect the fracture surface to ensure that the fluid in the wet region does not leak to the dry region.

The larger compliance values indicate that the P-P reflection coefficients are larger than those in the previous experiments. Using a more viscous fluid introduces the additional effects of viscosity in the reflection coefficients. However, the theoretical and experimental studies of a thin layer filled with a viscous fluid (Rokhlin and Wang, 1991; Zhu et al., 2011) predict that the increase of viscosity decreases the P-P reflection coefficients. As pointed out in Minato and Ghose (2016a), the inclusion of air in the water increases the P-P reflection coefficients. Because the viscosity of hair gel is also exploited in the acoustic experiments of air bubbles (Leroy et al., 2008), here we discuss the possibility that the amount of air bubbles trapped in the fluid is larger than that in the previous experiments. For this purpose, we assume that the estimated aperture in the previous experiments (the residual aperture plus the spacer thickness) represents the true aperture, and we estimate the effective bulk modulus of the fluid in the present experiments.

We consider the following model:

$$\eta_N^{-1} = K_{\text{eff}}/d, \tag{4}$$

where K_{eff} is the effective bulk modulus of the fluid. We assume that the effective fracture aperture d is 140 μm, which is derived in

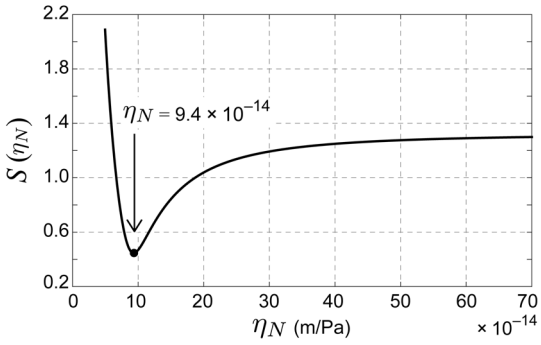

Figure 5. The misfit function (equation 3) in estimating the normal compliance from the observed reflection coefficients (Figure 4).

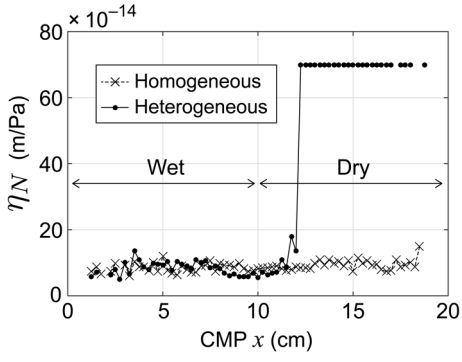

Figure 6. The estimated values of the normal compliance at each CMP for the homogeneously wet fracture (crosses) and the heterogeneously wet fracture (filled circles). The wet and dry regions in the heterogeneously wet fracture are shown.

the previous experiments (Minato and Ghose, 2016a). Assuming this value of the fracture aperture, in this study, we obtain the effective bulk modulus of the fluid at the wet region to be $K_{\text{eff}} = 1.42 \times 10^9$–$1.78 \times 10^9$ Pa. As we discussed above, we consider the inclusion of a small amount of air bubbles in water in order to explain the effective bulk modulus. In this study, we use the linear-slip model, which assumes a large wavelength and the continuity of stress across a thin layer. Therefore, we consider the effective bulk modulus derived from a simple iso-stress averaging for a two-phase medium (Reuss average, Mavko et al., 2009):

$$K_{\text{eff}}^{-1} = f_A/K_A + (1 - f_A)/K_W, \tag{5}$$

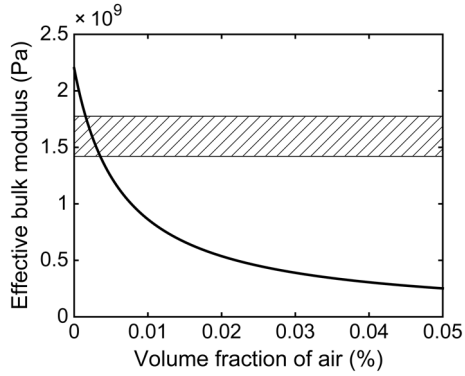

Figure 7. The effective bulk modulus of the mixture of water and air (Reuss average). The hatched area shows the values of the bulk modulus obtained in this study.

where K_A is the bulk modulus of air (1.42×10^5 Pa), K_W is that of water (2.2×10^9 Pa), and f_A is the volume fraction of air. Using equation 5, the effective bulk modulus K_{eff} as a function of the volume fraction of air f_A is calculated (Figure 7). Considering that the detected bulk modulus is 1.42×10^9–1.78×10^9 Pa, the expected amount of air bubbles is 1.6×10^{-3}–3.5×10^{-3}%. These values of volume fraction of air bubbles are similar to those considered in sediments (van Dalen et al., 2010). We conclude that the values of the normal compliance of the fracture obtained from the AVO inversion (Figure 6) are reasonable.

Finally, we check the thickness of the fracture with respect to the used seismic wavelength in our experiment. Given the observed predominant frequency of the reflections to be 0.7 MHz and $V_P = 6400$ m/s, the wavelength of the P-wave is approximately 0.9 cm. The total thickness of the fracture is 140 μm, as discussed above. Therefore, the wavelength is approximately 65 times larger than the fracture thickness. It is significant that the compliance of such a thin fracture relative to the wavelength can still be sensed by the seismic waves.

Effects of scattering due to spatially varying compliance

Spatial heterogeneity has been shown numerically to lead to the generation of scattered waves (Nakagawa et al., 2004). The heterogeneously wet fracture in our experiments contains a sharp lateral change in compliance at the boundary between the wet and the dry region at the fracture (at $x = 10$ cm). This boundary may behave as a point scatterer producing waves that do not obey the Snell's law (Figure 8a).

Using the known values of source and receiver locations, we calculate the traveltime of specular reflections T_{PP} and that of the scattered waves T_{Sc} for the shot gather with the source at $x = 16$ cm (Figure 8b). Here, we consider only P-P scattered waves. Figure 8c and 8d shows the difference between the homogeneously wet fracture response and the dry response, and that between the heterogeneously wet fracture response and the dry response, respectively.

One can clearly see that the amplitude of the residual energy (difference) in Figure 8c shows smooth variation along the traveltimes of the specular reflections (see the red color and T_{PP} in Figure 8c). This indicates that the specular reflections are dominant in the homogeneously wet fracture response. Please also note that the apparent traveltime delay of the residuals (the red color) from T_{PP} in Figure 8c corresponds to the apparent traveltime delay for the peak amplitude of the wavelet (see Figure 8b). On the other hand, the large residual energy (blue and red color) in Figure 8d is located around the traveltimes of the scattered waves T_{Sc}, especially at approximately $x = 80$–120 mm (the red ellipse in Figure 8d). This indicates the presence of scattered waves in the heterogeneously wet fracture response.

Depending on source and receiver geometry, the specular reflections (signals for AVO inversion) are interfered by scattered waves. To check their effects, we apply the same inversion pro-

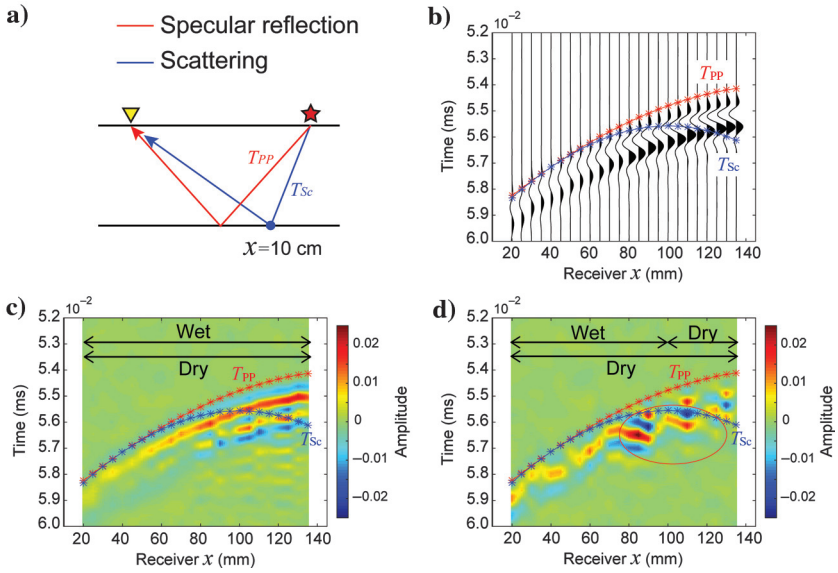

Figure 8. (a) Schematic figure showing a specular reflection (traveltime T_{PP}) and a scattered wave (traveltime T_{Sc}) generated at a sharp lateral change in fracture compliance ($x = 10$ cm) and (b) the observed shot gather (source at $x = 16$ cm) for the dry fracture with receivers located between $x = 2$ and $x = 14$ cm. The estimated traveltimes (T_{PP} and T_{Sc}) are shown. (c) The difference between the homogeneously wet fracture response and the dry fracture response. The wet region and dry region in the two responses are shown. (d) The same as (c) but for the difference between the heterogeneously wet fracture response and the dry fracture response.

cedure again but using each trace at the CMP gathers. We obtain the normal compliances (Figure 9a and 9b). The values of the compliance show fluctuations and a few spikes, probably because of the single-trace inversion providing less-constrained solutions than the multitrace AVO inversion. Nevertheless, it clearly distinguishes the dry region from the wet region along the fracture (compare Figure 9a and 9b).

We calculate the traveltime difference between the predicted specular reflections and the predicted scattered waves ($T_D = T_{Sc} - T_{PP}$) at each trace in the CMP gathers (Figure 9c). The specular reflections with wavelengths larger than the time differences (Figure 9c) interfere with the scattered waves. Assuming that Figure 9c shows the maximum window lengths that can capture the specular reflections without the interference of the scattered waves, their inverse (T_D^{-1}) gives approximate values for the minimum frequencies that are not affected by the scattered waves. Considering the fact that the maximum frequency that we use for the inversion to be approximately 1.6 MHz (Figure 4), the data at CMP $x = 8$–12 cm may be more contaminated by the scattered waves than data at other CMP locations (see Figure 9d). This is likely to be the reason why we obtain the boundary of the sharp change in compliance slightly shifted at CMP $x = 12$ cm compared to the true location of the boundary (Figures 6 and 9b).

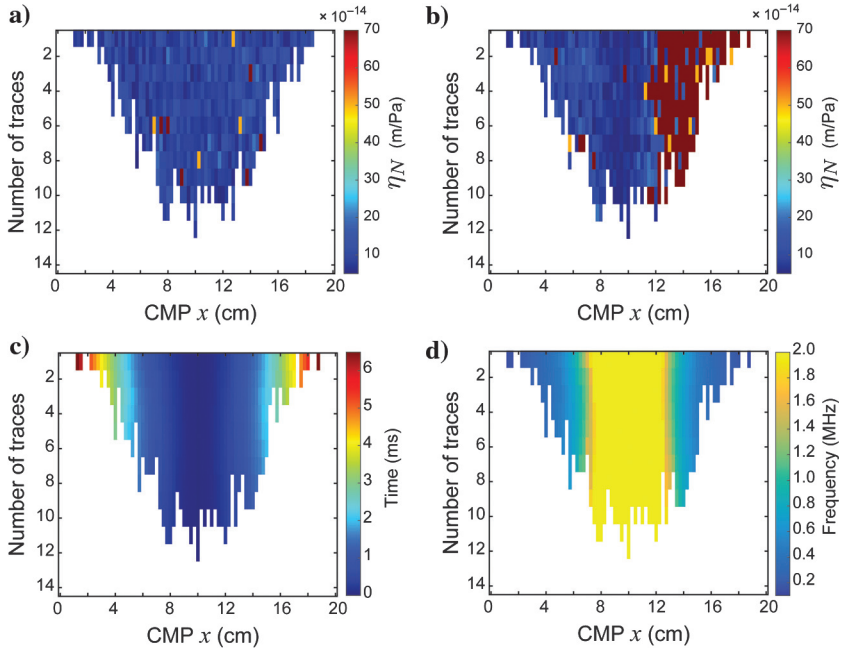

Figure 9. Estimated normal compliance η_N at each trace in the CMP gathers for (a) a homogeneously wet fracture and (b) a heterogeneously wet fracture; (c) the predicted traveltime difference between the specular reflections and the scattered waves ($T_D = T_{Sc} - T_{PP}$); and (d) the approximate value for the minimum frequencies that do not interfere with the scattered waves. The values are clipped at 2 MHz.

Note that the compliance values at the wet region (CMP $x = 1$–10 cm) of the heterogeneously wet fracture (Figure 9b) are similar to those for the homogeneously wet fracture (Figure 9a), which do not contain the scattered waves, suggesting that the effect of the scattered wave is small at the wet region. This is probably because of the radiation pattern of the scattering. It will require additional laboratory tests and numerical modeling to ascertain the amplitude of the scattered waves. Furthermore, an inverse scattering approach (Minato and Ghose, 2014, 2016b), which exploits the scattering due to the heterogeneous compliance, may improve the estimation of the compliance distribution, although it will require additional processing for the wavefield extrapolation.

In this study, we consider only quasistatic effects without fluid flow in a fracture. However, laterally propagating waves along a fluid-filled fracture (small-strain lateral fluid flow) are extensively reported (Tang and Cheng, 1989; Korneev, 2008). Recent research shows the possibility of generation of these waves due to the passage of elastic waves at the tip of a fracture (Derov et al., 2008; Frehner, 2014) and in an open fracture intersecting a borehole (Minato and Ghose, 2017). Similar to tube-wave generation models (Ionov, 2007; Bakku et al., 2013) in which the fluid flow is generated due to the deformation of a fracture and due to the boundary conditions at the edges of the fracture, the lateral boundary at the center of the fracture in our experiments (drained/undrained) can cause differences in the behavior of the laterally propagating waves in the fracture. This effect may be represented by different values of the fracture compliances around the center of the fracture in the homogeneously wet fracture and in the heterogeneously wet fracture. In this vein, several previous studies attempt to incorporate the effect of fluid flow into the linear-slip model (Nakagawa and Schoenberg, 2007; Barbosa et al., 2017) and discuss a relation between fracture compliances and the Krauklis waves in a fracture (Nakagawa and Korneev, 2014). Changes in the fracture compliances around the center of the fracture due to the laterally propagating waves also contribute to the generation of scattered waves. The effects of scattered waves are discussed in this subsection. The fact that the estimated fracture compliances at the wet region in the homogeneously wet fracture (CMP $x = 0$–10 cm) are similar to those in the heterogeneously wet fracture (Figure 6) implies that the effect of scattering due to laterally propagating waves may not be large in our experiments.

CONCLUSION

We perform ultrasonic laboratory experiments to characterize the spatially varying compliance along a fluid-filled fracture. We simulate in the laboratory surface seismic or borehole measurements involving multiple sources and receivers. We carry out AVO inversion of the CMP gathers, considering the linear-slip model for the fractures, to estimate theoretically the reflection response. The estimated compliance distribution distinguishes clearly the dry region from the wet region of the fracture even when the seismic wavelength is approximately 65 times larger than the thickness of the fracture.

The effective bulk modulus of the fluid (fracture infill) is obtained from the estimated values of the fracture compliance. The obtained bulk modulus can be quite well-explained by the presence of minute quantities of air bubbles in water. We find new evidence for scattered waves due to a sharp lateral change in compliance along the fracture. The detected boundary between the dry and the wet regions of the fracture is slightly shifted in our estimate compared with the

true location, possibly due to the interference of the scattered waves generated at the boundary.

Because the linear-slip model can represent various thin structures in rocks at different scales, these findings can be instrumental in developing many new applications, e.g., in deep and shallow seismic explorations and in nondestructive material testing.

ACKNOWLEDGMENTS

We thank the three anonymous reviewers for their helpful reviews and constructive comments. We thank K. Heller for his assistance in laboratory experiments. This work is supported by The Netherlands Research Centre for Integrated Solid Earth Science (ISES).

REFERENCES

Acosta-Colon, A., L. J. Pyrak-Nolte, and D. D. Nolte, 2009, Laboratory-scale study of field of view and the seismic interpretation of fracture specific stiffness: Geophysical Prospecting, **57**, 209–224, doi: 10.1111/j.1365-2478.2008.00771.x.

Aydin, A., 2000, Fractures, faults, and hydrocarbon entrapment, migration and flow: Marine and Petroleum Geology, **17**, 797–814, doi: 10.1016/S0264-8172(00)00020-9.

Baird, A., J. Kendall, and D. Angus, 2013, Frequency-dependent seismic anisotropy due to fractures: Fluid flow versus scattering: Geophysics, **78**, no. 2, WA111–WA122, doi: 10.1190/geo2012-0288.1.

Bakku, S. K., M. Fehler, and D. Burns, 2013, Fracture compliance estimation using borehole tube waves: Geophysics, **78**, no. 4, D249–D260, doi: 10.1190/geo2012-0521.1.

Bakulin, A., V. Grechka, and I. Tsvankin, 2000, Estimation of fracture parameters from reflection seismic data — Part I: HTI model due to a single fracture set: Geophysics, **65**, 1788–1802, doi: 10.1190/1.1444863.

Barbosa, N. D., J. G. Rubino, E. Caspari, and K. Holliger, 2017, Extension of the classical linear slip model for fluid-saturated fractures: Accounting for fluid pressure diffusion effects: Journal of Geophysical Research: Solid Earth, **122**, 1302–1323, doi: 10.1002/2016JB013636.

Chaisri, S., and E. S. Krebes, 2000, Exact and approximate formulas for P-SV reflection and transmission coefficients for a nonwelded contact interface: Journal of Geophysical Research: Solid Earth, **105**, 28045–28054, doi: 10.1029/2000JB900296.

Derov, A. V., G. A. Maximov, and M. Y. Lazarkov, 2008, On boundary condition at tips of fluid filled fracture for description of the slow fracture mode generation by external acoustical field the effective boundary condition of the mixed, *in* O. V. Rudenko, A. V. Korchak, and S. N. Gurbatov, eds., Proceedings of the XX Session of the Russian Acoustical Society: Russian Acoustical Society, 184–186.

Frehner, M., 2014, Krauklis wave initiation in fluid-filled fractures by seismic body waves: Geophysics, **79**, no. 1, T27–T35, doi: 10.1190/geo2013-0093.1.

Gu, B., R. Suárez-Rivera, K. T. Nihei, and L. R. Myer, 1996, Incidence of plane waves upon a fracture: Journal of Geophysical Research, **101**, 25337–25346, doi: 10.1029/96JB01755.

Hopkins, D. L., N. G. Cook, and L. R. Myer, 1987, Fracture stiffness and aperture as a function of applied stress and contact geometry: Presented at the 28th US Symposium on Rock Mechanics (USRMS), American Rock Mechanics Association, 673–680.

Hudson, J. A., E. Liu, and S. Crampin, 1997, The mean transmission properties of a fault with imperfect facial contact: Geophysical Journal International, **129**, 720–726, doi: 10.1111/j.1365-246X.1997.tb04507.x.

Ionov, A. M., 2007, Stoneley wave generation by an incident P-wave propagating in the surrounding formation across a horizontal fluid-filled fracture: Geophysical Prospecting, **55**, 71–82, doi: 10.1111/j.1365-2478.2006.00577.x.

Kame, N., K. Nagata, M. Nakatani, and T. Kusakabe, 2014, Feasibility of acoustic monitoring of strength drop precursory to earthquake occurrence: Earth, Planets and Space, **66**, 41, doi: 10.1186/1880-5981-66-41.

Korneev, V., 2008, Slow waves in fractures filled with viscous fluid: Geophysics, **73**, no. 1, N1–N7, doi: 10.1190/1.2802174.

Lavrentyev, A. I., and S. I. Rokhlin, 1998, Ultrasonic spectroscopy of imperfect contact interfaces between a layer and two solids: Journal of the Acoustical Society of America, **103**, 657–664, doi: 10.1121/1.423235.

Lee, S. H., M. F. Lough, and C. L. Jensen, 2001, Hierarchical modeling of flow in naturally fractured formations with multiple length scales: Water Resources Research, **37**, 443–455, doi: 10.1029/2000WR900340.

Leroy, V., A. Strybulevych, J. H. Page, and M. G. Scanlon, 2008, Sound velocity and attenuation in bubbly gels measured by transmission experiments: Journal of the Acoustical Society of America, **123**, 1931–1940, doi: 10.1121/1.2875420.

Liu, E., J. A. Hudson, S. Crampin, W. D. Rizer, and J. H. Queen, 1995, Seismic properties of a general fracture, *in* H. P. Rossmanith, ed., Mechanics of jointed and faulted rock: A. A. Balkema Publishers, 673–678.

Lubbe, R., J. Sothcott, M. Worthington, and C. McCann, 2008, Laboratory estimates of normal and shear fracture compliance: Geophysical Prospecting, **56**, 239–247, doi: 10.1111/j.1365-2478.2007.00688.x.

Mavko, G., T. Mukerji, and J. Dvorkin, 2009, The rock physics handbook: Tools for seismic analysis of porous media: Cambridge University Press.

Minato, S., and R. Ghose, 2013, Inverse scattering solution for the spatially heterogeneous compliance of a single fracture: Geophysical Journal International, **195**, 1878–1891, doi: 10.1093/gji/ggt348.

Minato, S., and R. Ghose, 2014, Imaging and characterization of a subhorizontal non-welded interface from point source elastic scattering response: Geophysical Journal International, **197**, 1090–1095, doi: 10.1093/gji/ggu037.

Minato, S., and R. Ghose, 2015, Nonlinear imaging condition and the effect of source illumination: Imaging fractures as nonwelded interfaces: Geophysics, **80**, no. 2, A25–A30, doi: 10.1190/geo2014-0406.1.

Minato, S., and R. Ghose, 2016a, AVO inversion for a non-welded interface: estimating compliances of a fluid-filled fracture: Geophysical Journal International, **206**, 56–62, doi: 10.1093/gji/ggw138.

Minato, S., and R. Ghose, 2016b, Enhanced characterization of fracture compliance heterogeneity using multiple reflections and data-driven Green's function retrieval: Journal of Geophysical Research: Solid Earth, **121**, 2813–2836, doi: 10.1002/2015JB012587.

Minato, S., and R. Ghose, 2017, Low-frequency guided waves in a fluid-filled borehole: Simultaneous effects of generation and scattering due to multiple fractures: Journal of Applied Physics, **121**, 104902, doi: 10.1063/1.4978250.

Nagy, P., 1992, Ultrasonic classification of imperfect interfaces: Journal of Nondestructive Evaluation, **11**, 127–139, doi: 10.1007/BF00566404.

Nakagawa, S., and V. A. Korneev, 2014, Effect of fracture compliance on wave propagation within a fluid-filled fracture: Journal of the Acoustical Society of America, **135**, 3186–3197, doi: 10.1121/1.4875333.

Nakagawa, S., K. T. Nihei, and L. R. Myer, 2004, Plane wave solution for elastic wave scattering by a heterogeneous fracture: Journal of the Acoustical Society of America, **115**, 2761–2772, doi: 10.1121/1.1739483.

Nakagawa, S., and M. A. Schoenberg, 2007, Poroelastic modeling of seismic boundary conditions across a fracture: Journal of the Acoustical Society of America, **122**, 831–847, doi: 10.1121/1.2747206.

Oliger, A., D. D. Nolte, and L. J. Pyrak-Nolte, 2003, Seismic focusing by a single planar fracture: Geophysical Research Letters, **30**, 1203, doi: 10.1029/2002GL016264.

Pyrak-Nolte, L., and J. Morris, 2000, Single fractures under normal stress: The relation between fracture specific stiffness and fluid flow: International Journal of Rock Mechanics and Mining Sciences, **37**, 245–262, doi: 10.1016/S1365-1609(99)00104-5.

Pyrak-Nolte, L., L. Myer, and N. Cook, 1990, Transmission of seismic waves across single natural fractures: Journal of Geophysical Research, **95**, 8617–8638, doi: 10.1029/JB095iB06p08617.

Pyrak-Nolte, L., and D. Nolte, 1992, Frequency dependence of fracture stiffness: Geophysical Research Letters, **19**, 325–328, doi: 10.1029/91GL03179.

Reshetnikov, A., S. Buske, and S. Shapiro, 2010, Seismic imaging using microseismic events: Results from the San Andreas Fault System at SAFOD: Journal of Geophysical Research: Solid Earth, **115**, B12324, doi: 10.1029/2009JB007049.

Rokhlin, S. I., and Y. J. Wang, 1991, Analysis of boundary conditions for elastic wave interaction with an interface between two solids: Journal of the Acoustical Society of America, **89**, 503–515, doi: 10.1121/1.400374.

Schoenberg, M., 1980, Elastic wave behavior across linear slip interfaces: Journal of the Acoustical Society of America, **68**, 1516–1521, doi: 10.1121/1.385077.

Shuey, R., 1985, A simplification of the Zoeppritz equations: Geophysics, **50**, 609–614, doi: 10.1190/1.1441936.

Tang, X., and C. Cheng, 1989, A dynamic model for fluid flow in open borehole fractures: Journal of Geophysical Research: Solid Earth, **94**, 7567–7576, doi: 10.1029/JB094iB06p07567.

van Dalen, K. N., R. Ghose, G. G. Drijkoningen, and D. M. Smeulders, 2010, In-situ permeability from integrated poroelastic reflection coefficients: Geophysical Research Letters, **37**, L12303, doi: 10.1029/2010GL043319.

Willis, M., D. Burns, R. Rao, B. Minsley, M. Toksöz, and L. Vetri, 2006, Spatial orientation and distribution of reservoir fractures from scattered seismic energy: Geophysics, **71**, no. 5, O43–O51, doi: 10.1190/1.2235977.

Worthington, M., and R. Lubbe, 2007, The scaling of fracture compliance: Geological Society, London, Special Publications 270, 73–82.

Worthington, M. H., and J. A. Hudson, 2000, Fault properties from seismic Q: Geophysical Journal International, **143**, 937–944, doi: 10.1046/j.1365-246X.2000.00315.x.

Zhu, J. B., A. Perino, G. F. Zhao, G. Barla, J. C. Li, G. W. Ma, and J. Zhao, 2011, Seismic response of a single and a set of filled joints of viscoelastic deformational behaviour: Geophysical Journal International, **186**, 1315–1330, doi: 10.1111/j.1365-246X.2011.05110.x.